

# Fluid Dynamic Models of Flagellar and Ciliary Beating

ROBERT H. DILLON,<sup>a</sup> LISA J. FAUCI,<sup>b</sup> CHARLOTTE OMOTO,<sup>c</sup>  
AND XINGZHOU YANG<sup>d</sup>

<sup>a</sup>*Department of Mathematics, Washington State University, Pullman, Washington, USA*

<sup>b</sup>*Department of Mathematics, Tulane University, New Orleans, Louisiana, USA*

<sup>c</sup>*School of Biological Sciences, Washington State University, Pullman, Washington, USA*

<sup>d</sup>*Center for Computational Science, Tulane University, New Orleans, Louisiana, USA*

**ABSTRACT:** We have developed a fluid–mechanical model of a eucaryotic axoneme that couples the internal force generation of dynein molecular motors, the passive elastic mechanics of microtubules, and forces due to nexin links with a surrounding incompressible fluid. This model has been used to examine both ciliary beating and flagellar motility. In this article, we show preliminary simulation results for sperm motility in both viscous and viscoelastic fluids, as well as multiciliary interaction with a mucus layer.

**KEYWORDS:** immersed boundary method; sperm motility; cilia; mucus transport

## INTRODUCTION

Sperm motility and ciliary beating are vital ingredients of successful mammalian reproduction (see Ref. 1 for review). Sperm exhibit a variety of beat forms on the journey toward the oocyte. These waveforms are an emergent property of the interaction between the flagella's internal force generating mechanisms, the passive elastic structure of the axoneme, and the external fluid dynamics. These flagellar beat forms include a symmetric sinusoidal-like waveform as well as various asymmetric patterns of hyperactivated sperm in Newtonian and complex fluid environments. Ho and Suarez<sup>2</sup> and Katz *et al.*<sup>3</sup> investigated the swimming dynamics of human sperm in cervical mucus. In mucus, the bends were confined to the distal portion of the flagella

Address for correspondence: Robert H. Dillon, Department of Mathematics, Washington State University, Pullman, Washington 99164, USA.  
dillon@math.wsu.edu

Ann. N.Y. Acad. Sci. 1101: 494–505 (2007). © 2007 New York Academy of Sciences.  
doi: 10.1196/annals.1389.016

and show lower amplitude and wavelength compared to those expressed in a Newtonian fluid.

The mathematical modeling of sperm motility and ciliary motion has a rich history beginning with the pioneering works of Taylor,<sup>4</sup> Gray and Hancock,<sup>5</sup> and Lighthill<sup>6</sup> and more recent contributions by many others (for review, see Ref. 1). The mathematical approaches include resistive force theories,<sup>7-9</sup> slender body and boundary element methods,<sup>6,10-13</sup> and immersed boundary methods.<sup>14,15</sup> Fulford *et al.*<sup>16</sup> presented an analysis of flagellar motility in a viscoelastic fluid. This was based on a resistive force model of small-amplitude waves in a linear viscoelastic Maxwell fluid. In their analysis for a fixed flagellar beat form, the swimming velocity was the same for both the Newtonian and Maxwell fluids. However, the rate of work decreases as the elasticity increases. Thus, for a fixed rate of work, higher swimming velocities might be possible as the elasticity increased.

Ciliary motion is also an important feature of reproduction. For example, oviductal cilia play an important role in ovum pickup by the oviduct,<sup>17</sup> and ovum transport within the oviduct.<sup>18</sup> Since the structure of the axoneme is virtually identical in cilia and spermatazoa, it is appropriate to develop mechanical models for cilia and sperm concurrently. There remain a variety of open questions in ciliary and sperm mechanics: What governs the activation of dyneins to produce the wide variety of flagellar and ciliary waveforms? What are the mechanisms governing multiciliary waveforms? What is the mechanical basis for hyperactivation of sperm and what is the steering mechanism for sperm in those species that are chemotactic? We believe that an accurate representation of the surrounding fluid mechanics is essential to address these questions.

## MATHEMATICAL MODEL AND NUMERICAL METHOD

The motion of eucaryotic cilia and flagella is governed by an elaborate internal structure, the axoneme, which is powered by dynein molecular motors distributed regularly along its length and circumference. A cross-section of the axoneme consists of a central pair of singlet microtubules surrounded by nine outer doublet microtubules and encased by the cell membrane.<sup>19,20</sup> The bending of the axoneme is caused by sliding between pairs of outer doublets. Active sliding is due to the unidirectional ATP-induced force generation of the dynein power stroke. Backward, passive sliding is due to the active sliding of other pairs of doublets within the axoneme. The precise nature of the spatial and temporal control mechanisms regulating the various flagellar and ciliary beats is still unknown.<sup>21</sup> Considerable interest has been focused on understanding how the local force production of the dynein motors is translated into the controlled, regular beating of the global structure (for example, see Refs. 22 and 23).

We have developed a model for cilia and flagella that incorporates discrete representations of the dynein arms, the passive elastic structure of the axoneme including the doublets and nexin link.<sup>14,15,24</sup> Detailed geometric information is available, such as the spacing and shear between the microtubules, the local curvature of individual microtubules, and the stretching of the nexin links. In addition, the explicit representation of the dynein motors has allowed us the flexibility to incorporate a variety of dynein activation mechanisms. In a simple 2D model, the dyneins are represented by dynamic, diagonal links connecting two adjacent microtubules that make up the cilium or flagellum. Contraction of activated dyneins generates sliding between the two microtubules. One end of the dynein can attach, detach, and reattach to attachment sites on the microtubule.

The immersed boundary method, originally developed by Peskin to model blood flow in the heart,<sup>25–27</sup> provides a framework for coupling elastic dynamics of flexible boundaries with a surrounding viscous, incompressible fluid. While traditionally used in the context of biological applications (e.g., Refs. 28–31,14), the immersed boundary method is now considered a classical method in computational fluid dynamics, and has impacted nonbiological applications.<sup>32</sup> In an immersed boundary framework, elastic objects are accounted for by suitable contributions to a force term in the fluid dynamics equations. The force of each object on the fluid is a Dirac delta function layer of force supported only by the region of fluid that coincides with material points of the object. Once these forces on the fluid are accounted for, one can solve the fluid dynamics equations on a finite difference or finite element grid.

The structure of our 2D model axoneme consists of microtubules (see FIG. 1). Each of the axoneme's two microtubules consists of two filaments with diagonal cross-links. These filaments are the immersed elastic structures that will exert force on the surrounding fluid. The filaments are highly resistant to stretching and compression but offer no resistance to bending.

Resistance to bending of the microtubules is governed by the elastic properties of the diagonal cross-links. Adjacent pairs of microtubules are interconnected with horizontal links representing the nexin links of the

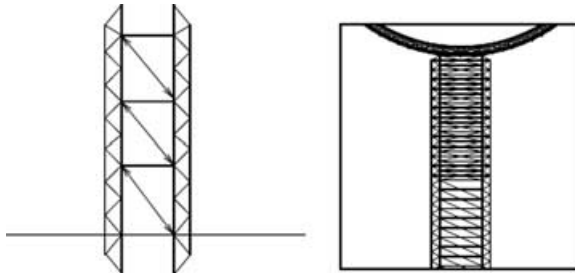


**FIGURE 1.** Detail of model sperm axoneme showing the basal body and head.

axoneme. Dynein motors are represented as dynamic diagonal elastic links between adjacent pairs of microtubules. These elastic springs may form, change connectivity, and may be broken during the course of the simulations. Dynamic link formulations have been used in other immersed boundary calculations to model cell–cell cohesion in platelet aggregation<sup>28</sup> and biofilm formation.<sup>33</sup> In addition, dynamic links have been used to simulate a viscoelastic fluid within the immersed boundary framework.<sup>34</sup>

In cilia and flagella, the active sliding between adjacent pairs of microtubules can occur in only one direction. Thus, dyneins on different pairs of microtubules must be activated to produce a ciliary or flagellar beat. We accomplish this in our model by allowing two configurations. In the *left to right* configuration shown in the schematic, designated *LR mode*, the dyneins are permanently attached to fixed nodes on the left microtubule. Dynein attachment on the opposite microtubule attachment sites can be transitory. Contraction of the dynein generates sliding between the two microtubules with the right-hand microtubule moving upward relative to the left. Since the pair of microtubules is tethered at the base, sliding is converted to bending and the tip moves toward the right. In the *right to left* configuration, designated *RL mode* (not shown), the dyneins are permanently attached to fixed nodes on the right-hand microtubule and extend downward toward transitory attachment sites on the left-hand microtubule. As the dyneins contract, the left-hand microtubule moves upward relative to the right-hand microtubule and the tip moves toward the left. In either configuration, one end of a dynein can attach, detach, and reattach to attachment sites on the microtubule. In our model of flagellar swimming, some of the dyneins are in *LR mode* and others in *RL mode*.

A structure representing the cell body may be included. The model for the sperm axoneme includes a specialized basal region adjacent to the cell body as shown in FIGURE 1 (right). The model basal body includes a network of elastic elements extending from one microtubule to the other, which are designed to restrict relative movement between the two microtubules. Dyneins and nexin links are deleted from this basal region. Although cilia also have basal bodies in the region near the cell wall, this has not yet been included in the cilia models.

The crucial feature of this fluid–structure interaction model is that the axoneme is not the computational boundary in the Navier–Stokes solver. This immersed boundary is the source of a dynamic force field that influences the fluid motion through the force term in the fluid equations. A discrete delta function communicates information between the fluid domain and the immersed boundary points. This allows us to easily simulate the interaction of several cilia or sperm efficiently. Since the computational domain is a fixed rectangle, we can use an efficient fluid solver designed for a regular grid with simple boundary conditions. We use a finite difference scheme with periodic boundary conditions for the fluid equations. This method, described in detail in Ref. 35 is a fast fourier transform method suited for low Reynolds numbers.

## THRESHOLD MODEL

Motivated by Brokaw,<sup>7</sup> we have implemented curvature-controlled dynein activation models.<sup>14,15,24</sup> In the Threshold model presented here, a dynein mode switches from *RL* to *LR* if the local curvature exceeds a specified positive threshold value *TH*. Similarly, the dynein switches from *LR* to *RL* mode when the local curvature falls below a specified negative threshold value—*TH*. Once the mode is switched, the activation of the dynein is delayed by a time  $\tau$ . The curvature at each of the dynein locations along the axoneme is calculated using splines.<sup>36</sup> We have experimented with values of *TH* in the range of  $[0,6]$  *rads/m*  $\times 10^4$ . In all of the simulations shown here, we set *TH* = 3. In addition, each of the simulations begins with a sinusoidal curve and is run at a fixed viscosity of 1 cp for the first 300 frames (0.06 sec). By this time a regular flagellar beat is well established and the effects of viscosity changes can be readily observed. In FIGURE 2 we show profiles of the sperm at the 800th frame. In panel (A) the viscosity is held at 1 cp for the duration of the simulation. In panels (B), (C), and (D) the viscosity changes to 5 cp, 10 cp, and 15 cp at the 300th frame. The remaining parameters are identical in each simulation. In FIGURE 3, T we show shear plots of these simulations. The shear plots, which give the bend angle along the length of the flagella, are generated over time frames that give approximately one full ciliary beat for each plot. In these simulations increasing viscosity results in flagellar waveforms of decreasing amplitude, decreasing wavelength, and lower swimming velocities.

## LAGRANGIAN MESH METHODS

The rheology of complex fluids is quite diverse, but some, such as mucus, incorporate a hydrated polymer matrix. The rheological properties of mucus depend not only on the concentration of polymers in the mucus gel, but also on the nature of the interconnections of the polymer chains in the mucus matrix. The mucin polymers are held together by tangles and low-energy bonds.<sup>37</sup> In Lagrangian mesh methods, the matrix can be modeled directly. Such a method

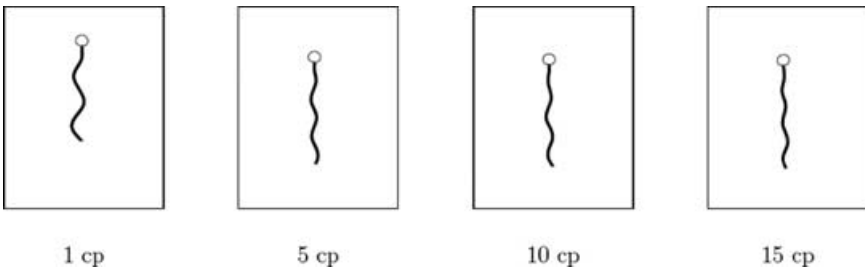
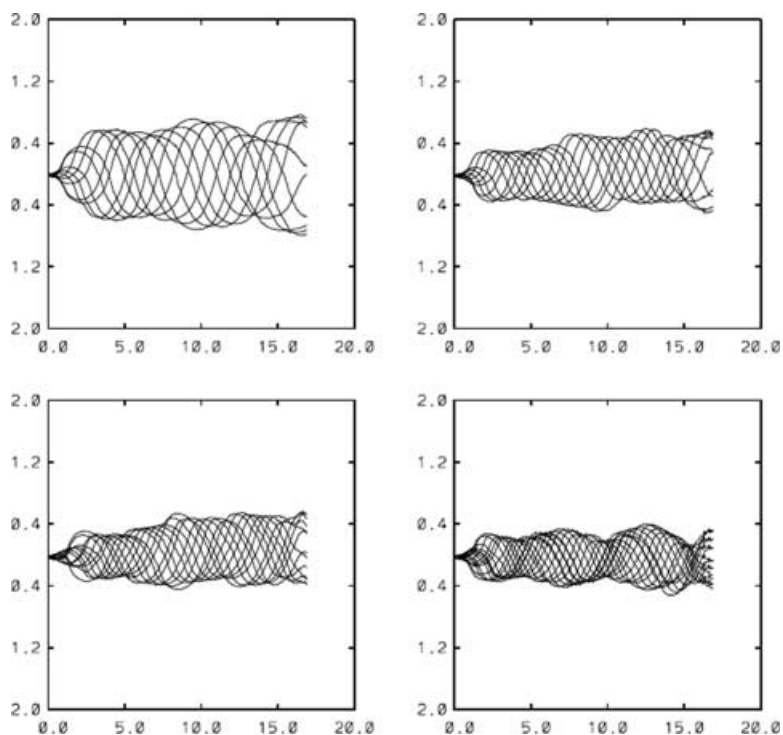


FIGURE 2. Threshold swimming profiles at increasing viscosity.



**FIGURE 3.** Shear plots of threshold model at viscosities 1 cp (upper left), 5 cp (upper right), 10 cp (lower left), and 15 cp (lower right).

was introduced by Bottino<sup>38</sup> for modeling the actin cytoskeleton by means of a network of nodes that could be cross-linked with viscoelastic links. The initial location of the nodes was chosen randomly and viscoelastic links between them could form or break. The evolution of the link connections could depend on the temporal history of the links. Bottino studied the macroscopic properties of the complex fluid as a property of these microscopic rules through several numerical rheological experiments.

Here, we describe a preliminary version of a Lagrangian Mesh network for modeling complex fluids, such as mucus. The mesh is represented as a discrete set of immersed boundary points, which are connected via viscoelastic links. Deformation of the mesh produces forces that are introduced into the Stokes or Navier–Stokes equation. The mesh is initialized as a regular grid. In a 2D mesh, each node is connected to its nearest neighbors in both the vertical, horizontal, and diagonal directions. Link ages between adjacent nodes incorporate discrete viscoelastic elements. In the simulations shown here, a Jeffreys element was employed for the viscoelastic links. This consists of Voigt element (spring and viscous dashpot in parallel) connected in series with a viscous dashpot. For a

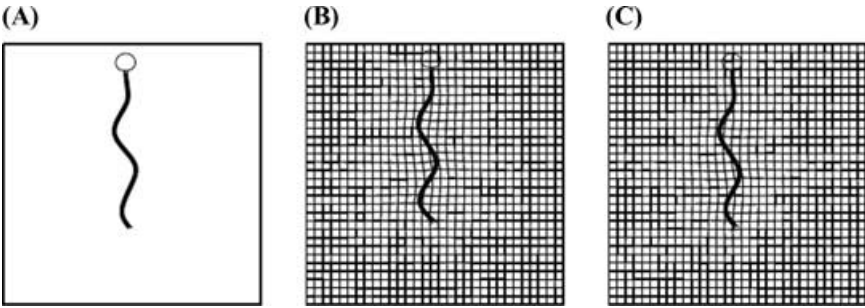


**FIGURE 4.** Viscoelastic profiles at same time frame for threshold model. (A) No mesh with  $cp = 1$ . (B) Lagrangian mesh with  $cp = 1$ , Stiffness = 10,  $\mu_1 = \mu_2 = 1$ . (C) Lagrangian mesh with  $cp = 1$ , Stiffness = 5,  $\mu_1 = \mu_2 = 1$ .

single Jeffreys element connecting mesh points  $P_1$  and  $P_2$ , we let  $x = \|P_2 - P_1\| = x_1 + x_2 + L$  where  $x_1$  is the extension of the spring,  $x_2$  is the creep length, and  $L$  is the spring resting length. In the Jeffreys element, since the Voigt element is in series with the dashpot, the force produced by the Voigt element equals the force produced by the dashpot. Thus

$$kx_1 + \mu_1 \dot{x}_1 = \mu_2 \dot{x}_2, \tag{1}$$

where  $k$  is the spring stiffness,  $\mu_j, j = 1, 2$ , are the dashpot drag coefficients. Since  $\dot{x} = \dot{x}_1 + \dot{x}_2$ , we can eliminate  $\dot{x}_2$  in Equation 1 and obtain

$$\mu \dot{x}_1 + \alpha x_1 = \dot{x} \tag{2}$$

where  $\alpha = \frac{k}{\mu_2}$  and  $\mu = \frac{\mu_1 + \mu_2}{\mu_2}$ . From this we can obtain a solution for  $\dot{x}_1$  in terms of  $\dot{x}$ :

A time  $t^n$  we have the locations for the Lagrangian mesh points  $P_1$  and  $P_2$ , we

1. Determine  $x^n = P_2 - P_1$
2. Determine  $\dot{x}^n \approx \frac{x^n - x^{n-1}}{\Delta t}$
3. Determine  $x_1^n$  and  $\dot{x}_1^n$
4. Determine the force at  $P_1$  and  $P_2$
5. Interpolate the Lagrangian mesh point forces to the Eulerian grid
6. Solve the Navier–Stokes equations
7. Move the mesh points at the local fluid velocity

The swimming of the sperm can produce significant deformation of the Lagrangian mesh. As a result, some form of mesh regriding is required. Here, we use a regriding method that tracks two separate Lagrangian grids. Each grid is reset to its initial configuration after a set time period. These reset times are staggered and the grid mesh forces averaged. Thus, the averaged mesh force contains the elastic deformation history over the mesh reset period.

We show, in FIGURE 4, snapshots of threshold swimming profiles with and without the Lagrangian mesh. Shear plots from these simulations are shown in FIGURE 5. As in the simulations shown in FIGURES 2 and 3, the simulations begin with a Newtonian fluid with fluid viscosity 1 cp. Midway through the simulation the mesh is introduced into the fluid domain. The profiles and shear plots are shown at the identical time frames in each of the simulations. In the range of parameter values for the stiffness constant and viscosity coefficients of the Lagrangian mesh shown here, the swimming profiles look very similar. However, the swimming speeds vary. The swimmer with the largest stiffness parameter, shown in FIGURES 4 and 5 panel (B), is swimming faster than the Newtonian swimmer in FIGURES 4 and 5 panel (A). The swimmer with a smaller stiffness parameter, but with increased mesh viscosity parameter  $\mu_1$ , shown in FIGURES 4 and 5 panel (C), is swimming slower than the Newtonian swimmer. As seen in the shear plots, the amplitude of the Lagrangian mesh swimmers is reduced in comparison with the Newtonian swimmer. These results are consistent with the finding by Fulford *et al.*<sup>16</sup> that sperm can swim faster in a Maxwell fluid with the same expenditure of energy as in a Newtonian fluid.

## CILIARY BEATING

Contaminating particles in the airways of the lung are cleared by mucociliary transport. Cilia, which line the airways, are covered by a thin layer of mucus, and beat in a coordinated manner to propel particles trapped in this mucus layer.<sup>39</sup> Scanning electron microscope images of cultured rabbit tracheal epithelium,<sup>40</sup> show individual, tightly packed, cilia propelling a mucus layer. Ciliary tips penetrate the mucus layer and push it in the direction of the power stroke.<sup>41</sup> During the recovery stroke, the cilia do not adhere to the mucus layer. This layer is viscoelastic, and exhibits finite yield stress, shear thinning, and thixotropy.<sup>42</sup> The fundamental interactions between the ciliated cells and the mucus layer are still poorly understood. It remains an open question as to how the internal

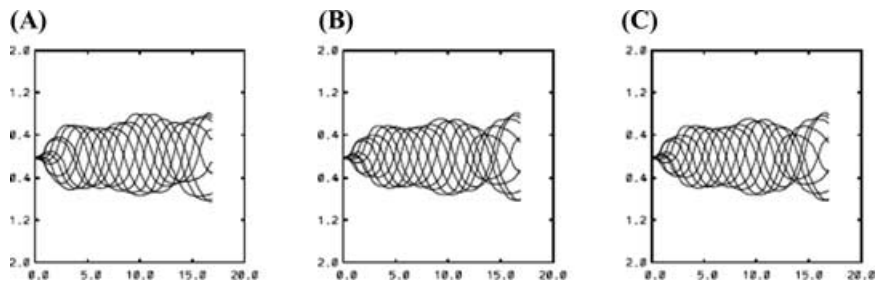


**FIGURE 5.** Shear plots from the simulations in FIGURE 4. (A) No mesh with  $cp = 1$ . (B) Lagrangian mesh with  $cp = 1$ , Stiffness = 10,  $\mu_1 = \mu_2 = 1$ . (C) Lagrangian mesh with  $cp = 1$ , Stiffness = 5,  $\mu_1 = \mu_2 = 1$ .

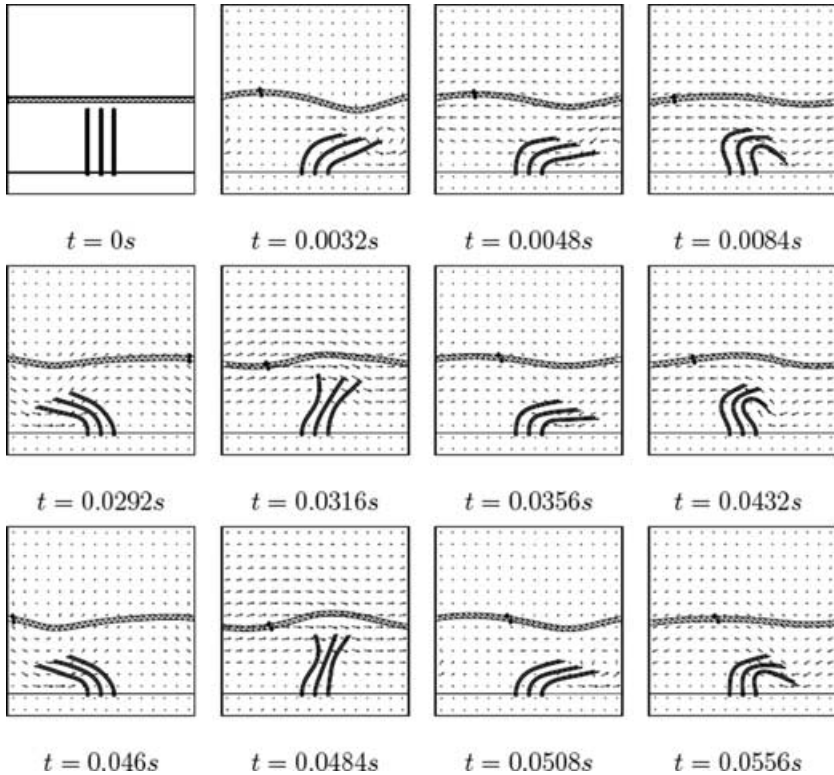


**FIGURE 6.** Transporting a mucus layer at selected times.

ciliary engine affects the ciliary beat form, and how this ciliary beat form influences the properties of mucus transport.

An immersed boundary model for multiciliary transport is described in detail in Yang *et al.*<sup>43</sup> Here we show preliminary results of a multiciliary simulation with the addition of a mucus layer modeled as an elastic mesh consisting of immersed boundary points connected by linear elastic elements.

In FIGURE 7 (upper row) we show simulation results in which the model parameters are identical to that in FIGURE 6 but without the mucus layer. A fictitious mucus layer is shown, but the points in the layer are treated in the simulation as fluid markers, which have no effect on the numerical solution. In FIGURE 7 (lower row) we show simulation results with the mucus layer at comparable stages of the ciliary beats. The cilia transporting a mucus layer beat more slowly than the cilia transporting just a Newtonian fluid. Moreover, as suggested by the fluid marker pattern in the upper simulation, there is more fluid mixing between the upper and lower layers of the fluid domain in the simulation without mucus.

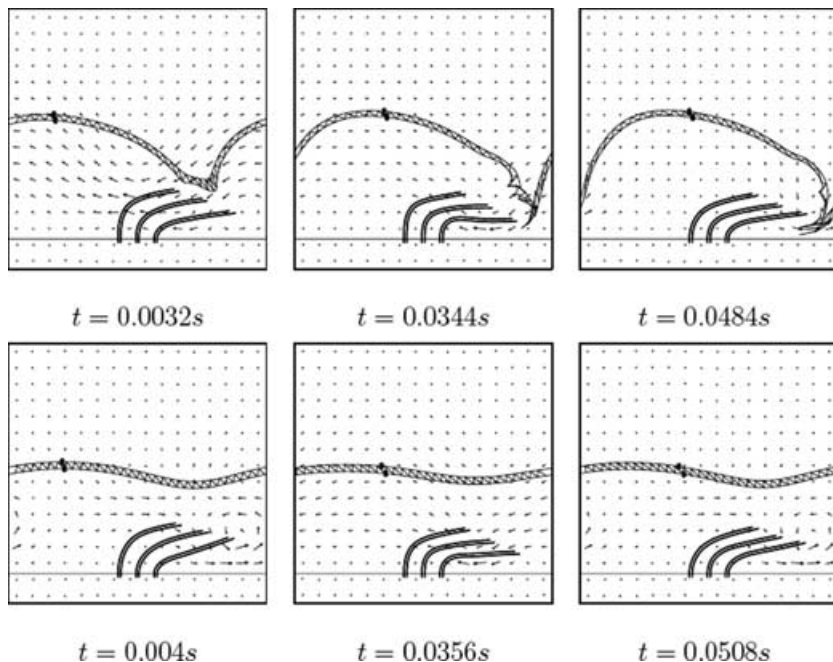


**FIGURE 7.** Comparison of ciliary transport with (lower) and without (upper) a mucus layer.

### DISCUSSION

All of the sperm simulations shown here are based on a Threshold curvature model for control of dynein activation. In the purely Newtonian fluid, we saw a consistent trend toward shorter wavelength, lower amplitude, and slower swimming velocities as the fluid viscosities increased. In the fluid, which included an overlying Lagrangian mesh, the Newtonian fluid viscosities were fixed at 1 cp. In these simulations compared to the Newtonian case, we saw little change in the flagellar wavelengths, significant decrease in flagellar amplitude, as well as lower and faster swimming velocities depending upon the Lagrangian mesh parameters. We are in the process of performing careful parameter studies in the context of this model.

### ACKNOWLEDGMENTS

This research has been supported by an NSF grant DMS-0201063. The simulations were run on SGI and AMD clusters at the Center of Computational Science, Tulane University, and Alpha and AMD computers at the Department of Mathematics, Washington State University.

## REFERENCES

1. FAUCI, L.J. & R. DILLON. 2006. Biofluid mechanics of reproduction. *Ann. Rev. Fluid Mech.* **38**: 371–394.
2. HO, H. & S. SUAREZ. 2001. Hyperactivation of mammalian spermatozoa: function and regulation. *Reproduction* **122**: 519–526.
3. KATZ, D., R. MILLS & T. PRITCHETT. 1978. The movement of human spermatazoa in cervical mucus. *Biol. Reprod.* **25**: 931–937.
4. TAYLOR, G.I. 1951. Analysis of the swimming of microorganisms. *Proc. R. Soc. Lond.* 447–461.
5. GRAY, J. & G. HANCOCK. 1955. The propulsion of sea-urchin spermatozoa. *J. Exp. Biol.* **32**: 802–814.
6. LIGHTHILL, J. 1976. Flagellar hydrodynamics. *SIAM Rev.* **18**: 161–230.
7. BROKAW, C.J. 1972. Computer simulation of flagellar movement. I. Demonstration of stable bend propagation and bend initiation by the sliding filament model. *Biophys. J.* **12**: 564–586.
8. HINES, M. & J.J. BLUM. 1978. Bend propagation in flagella. I. Derivation of equations of motion and their simulation. *Biophys. J.* **23**: 41–57.
9. HINES, M. & J.J. BLUM. 1979. Bend propagation in flagella. II. Incorporating of dynein cross-bridge kinetics into the equations of motion. *Biophys. J.* **25**: 421–442.
10. HIGDON, J. 1979. A hydrodynamic analysis of flagellar propulsion. *J. Fluid Mech.* **90**: 685–711.
11. HIGDON, J. 1979. The hydrodynamics analysis of flagellar propulsion: helical waves. *J. Fluid Mech.* **94**: 331–351.
12. HIGDON, J. 1979. The generation of feeding currents by flagellar motion. *J. Fluid Mech.* **94**: 305–330.
13. PHAN-THIEN, N., T. TRAN-CONG & M. RAMIA. 1987. A boundary-element analysis of flagellar propulsion. *J. Fluid Mech.* **184**: 533–549.
14. DILLON, R. & L.J. FAUCI. 2000. An integrative model of internal axoneme mechanics and external fluid dynamics in ciliary beating. *J. Theor. Biol.* **207**: 415–430.
15. DILLON, R., L.J. FAUCI & C. OMOTO. 2003. Mathematical modeling of axoneme mechanics and fluid dynamics in ciliary and sperm motility. *Dynam. Contin. Discrete Impuls. Systems: Series A* **10**: 745–757.
16. FULFORD, G.R., D.F. KATZ & R.L. POWELL. 1998. Swimming of spermatozoa in a linear viscoelastic fluid. *Biorheology* **35**: 295–309.
17. TALBOT, P., C. GEISKE & M. KNOLL. 1999. Oocyte pickup by the mammalian oviduct. *Mol. Biol. Cell* **10**: 5–8.
18. LENG, Z., D. MOORE, B. MUELLER, *et al.* 1998. Characterization of ciliary activity in distal fallopian tube biopsies of women with obstructive tubal infertility. *Hum. Reprod.* **11**: 3121–3127.
19. WITMAN, G.B. 1990. Introduction to cilia and flagella. *In* Ciliary and Flagellar Membranes. R.A. Bloodgood, Ed.: 1–30. Plenum. New York.
20. MURASE, M. 1992. *The Dynamics of Cellular Motility*. John Wiley. Chichester, UK.
21. BROKAW, C.J. 2001. Simulating the effects of fluid viscosity on the behavior of sperm flagella. *Math. Meth. Appl. Sci.* **24**: 1351–1365.
22. LINDEMANN, C.B. 1994. A ‘geometric clutch’ hypothesis to explain oscillations of the axoneme of cilia and flagella. *J. Theor. Biol.* **168**: 175–189.

23. BROKAW, C.J. 2005. Computer simulation of flagellar movement IX: oscillation and symmetry breaking in a model for short flagella and nodal cilia. *Cell Motil. Cytoskeleton* **60**: 35–47.
24. DILLON, R., L. FAUCI & X. YANG. 2006. Sperm motility and multiciliary beating: an integrative mechanical model. *Comp. Math. Appl.* **17**: 52: 749–758.
25. PESKIN, C.S. 1977. Numerical analysis of blood flow in the heart. *J. Comp. Phys.* **25**: 220–252.
26. PESKIN, C.S. 2002. The immersed boundary method. *Acta Numerica* **11**: 479–517.
27. PESKIN, C.S. & D.M. MCQUEEN. 1989. A three-dimensional computational method for bloodflow in the heart. I. Immersed elastic fibers in a viscous incompressible fluid. *J. Comput. Phys.* **81**: 372–405.
28. FOGELSON, A.L. 1984. A mathematical model and numerical method for studying platelet adhesion and aggregation during blood clotting. *J. Comp. Phys.* **56**: 111–134.
29. BEYER, R. 1992. A computational model of the cochlea using the immersed boundary method. *J. Comp. Phys.* **98**: 145–162.
30. ARTHURS, K.M., L.C. MOORE, C.S. PESKIN, *et al.* 1998. Modeling arteriolar flow and mass transport using the immersed boundary method. *J. Comp. Phys.* **147**: 402–440.
31. EGGLETON, C.D. & A.S. POPEL. 1998. Large deformation of red blood cell ghosts in a simple shear flow. *Phys. Fluids* **10**: 1834–1845.
32. MITTAL, R. & G. IACCARINO. 2005. Immersed boundary methods. *Ann. Rev. Fluid Mech.* **37**: 239–261.
33. DILLON, R., L.J. FAUCI, A. FOGELSON & D.P. GAVER. 1996. Modeling biofilm processes using the immersed boundary method. *J. Comp. Phys.* **129**: 57–73.
34. BOTTINO, D.C. 1998. Modeling viscoelastic networks and cell deformation in the context of the immersed boundary method. *J. Comp. Phys.* **147**: 86–113.
35. DILLON, R. & H.G. OTHMER. 1999. A mathematical model for outgrowth and spatial patterning of the vertebrate limb bud. *J. Theor. Biol.* **197**: 295–330.
36. DIERCKX, P. 1993. *Curve and Surface Fitting with Splines*. Oxford University Press. Oxford.
37. VERDUGO, P. 1998. Polymer biophysics of mucin cystic fibrosis. *In Proceedings of the International Congress on Cilia, Mucus, and Mucociliary Interactions*. G. Baum, Z. Priel, Y. Roth, N. Liron & E. Ostfeld, Eds.: 167–189. Marcel Dekker. New York.
38. BOTTINO, D.C. 1998. Modeling viscoelastic networks and cell deformation in the context of the immersed boundary method. *J. Comp. Phys.* **147**: 86–113.
39. GROTBORG, J. 1994. Pulmonary flow and transport phenomena. *Ann. Rev. Fluid Mech.* **26**: 529.
40. SANDERSONAND, M. & M. SLEIGH. 1981. Ciliary activity of cultured rabbit tracheal epithelium: beat pattern and metachrony. *J. Cell Sci.* **47**: 331.
41. GHEBER, L. & Z. PRIEL. 1998. Metachronal wave, ciliary stroke, and mucus propulsion. *In Cilia, Mucus, and Mucociliary Interactions*. G. Baum, Z. Priel, Y. Roth, N. Liron & E. Ostfeld, Eds.: 103. Marcel Dekker. New York.
42. STURGESS, J. 1977. Themucous lining of major bronchi in the rabbit lung. *Am. Rev. Resp. Dis.* **115**: 819.
43. YANG, X.-Z., R. DILLON & L. FAUCI. An integrative computational model of multiciliary beating. In preparation.